Validating gravitational-wave detections: The Advanced LIGO hardware injection system

C. Biwer,[1] J. Betzwieser,[2] R. P. Fisher,[1] E. Goetz,[3] S. Kandhasamy,[2] S. Karki,[4] J. S. Kissel,[3] A. P. Lundgren,[5] D. M. Macleod,[2] A. Mullavey,[2] K. Riles,[6] J. G. Rollins,[7] E. Thrane,[8] T. D. Abbott,[9] B. Allen,[5,10,11] D. A. Brown,[1] P. Charlton,[12] S. G. Crowder,[13] P. Fritschel,[14] J. B. Kanner,[7] C. Lazzaro,[15,16] M. Millhouse,[17] M. Pitkin,[18] R. L. Savage,[3] P. Shawhan,[19] D. H. Shoemaker,[14] J. R. Smith,[20] L. Sun,[21] J. Veitch,[22] S. Vitale,[14] A. J. Weinstein,[7] N. Cornish,[17] R. C. Essick,[14] M. Fays,[23] E. Katsavounidis,[14] J. Lange,[24] T. B. Littenberg,[25] R. Lynch,[14] P. M. Meyers,[26] F. Pannarale,[23] R. Prix,[5] R. O'Shaughnessy,[24] and D. Sigg[3]

[1]*Syracuse University, Syracuse, NY 13244, USA*
[2]*LIGO Livingston Observatory, Livingston, LA 70754, USA*
[3]*LIGO Hanford Observatory, Richland, WA 99354, USA*
[4]*University of Oregon, Eugene, OR 97403, USA*
[5]*Albert-Einstein-Institut, Max-Planck-Institut für Gravitationsphysik, D-30167 Hannover, Germany*
[6]*University of Michigan, Ann Arbor, MI 48109, USA*
[7]*LIGO, California Institute of Technology, Pasadena, CA 91125, USA*
[8]*Monash University, Victoria 3800, Australia*
[9]*Louisiana State University, Baton Rouge, LA 70803, USA*
[10]*University of Wisconsin-Milwaukee, Milwaukee, WI 53201, USA*
[11]*Leibniz Universität Hannover, D-30167 Hannover, Germany*
[12]*Charles Sturt University, Wagga Wagga, New South Wales 2678, Australia*
[13]*Bellevue College, Bellevue, WA 98008, USA*
[14]*LIGO, Massachusetts Institute of Technology, Cambridge, MA 02139, USA*
[15]*Center for Relativistic Astrophysics and School of Physics, Georgia Institute of Technology, Atlanta, GA 30332, USA*
[16]*INFN, Sezione di Padova, I-35131 Padova, Italy*
[17]*Montana State University, Bozeman, MT 59717, USA*
[18]*SUPA, University of Glasgow, Glasgow, G12 8QQ, United Kingdom*
[19]*University of Maryland, College Park, MD 20742, USA*
[20]*California State University Fullerton, Fullerton, CA 92831, USA*
[21]*The University of Melbourne, Parkville, Victoria 3010, Australia*
[22]*University of Birmingham, Birmingham, B15 2TT, United Kingdom*
[23]*Cardiff University, Cardiff CF24 3AA, United Kingdom*
[24]*Rochester Institute of Technology, Rochester, NY 14623, USA*
[25]*University of Alabama in Huntsville, Huntsville, AL 35899, USA*
[26]*University of Minnesota, Minneapolis, MN 55455, USA*

(Dated: November 15, 2016)

Hardware injections are simulated gravitational-wave signals added to the Laser Interferometer Gravitational-wave Observatory's (LIGO) data. The detectors' test masses are physically displaced by an actuator in order to simulate a gravitational wave. The simulated signal initiates a control-system response designed to mimic that of a true gravitational wave. Propagating a signal through the detector to the analyses provides an end-to-end test of LIGO's ability to observe gravitational waves. The gravitational-wave analyses used to detect and characterize signals are tested with hardware injections. By looking for discrepancies between the recovered and injected signals, we are able to characterize the performance of analyses and the coupling of subsystems to the detectors' output channels. Here we describe the LIGO hardware injection system and show the recovery of injected simulated signals from binary black hole mergers, a stochastic gravitational-wave background, isolated pulsars, and detector characterization studies.

I. INTRODUCTION

The Advanced Laser Interferometer Gravitational-Wave Observatory (aLIGO) is a network of two interferometric gravitational-wave detectors located in Hanford, WA, and Livingston, LA [1]. The aLIGO detectors are part of a global network of current and planned detectors including Virgo [2], GEO600 [3], KAGRA [4], and LIGO India [5]. The first direct observations of gravitational waves, both from binary black hole mergers, were made in aLIGO's first observing run [6, 7].

In order to to make confident statements about gravitational-wave events, aLIGO employs studies to understand both transient and persistent noise artifacts [8], and the calibration of the detectors [9, 10]. In addition, detection and parameter estimation analyses have techniques to mitigate non-Gaussian noise in the detectors' data [11, 12]. Testing these analyses and characterizing the detectors involves carrying out "hardware injections" in which simulated gravitational-wave signals are

added to the detector's output channel. Hardware injections have several uses. Following a detection candidate, we study similar simulated gravitational-wave signals through the use of repeated injections. These hardware injections provide an end-to-end check for the search and parameter estimation analyses to recover signals in the detectors' data. The recovery of hardware injections provides an additional check of the sign of the calibration between the aLIGO detectors using astrophysical waveforms and the recovery measures the time delay of the signal in the controls system; the calibration of the detectors is checked by other means as well [9, 10]. In addition, we can check for cross-couplings in the controls system to the detectors' output channel by identifying instrumental and environmental channels that are found to contain a trace of the injected signals.

Another use for hardware injection in Initial LIGO were "blind injections" which were hardware injections known only to a small team [13, 14]. Blind injections simulate the detection and characterization of a real astrophysical signal. No blind injections were carried out during aLIGO's first observing run.

aLIGO measures the differential displacement along the two arms $\Delta L = \delta L_x - \delta L_y$ but the output channel to analyses is gravitational-wave strain $h = \Delta L/L$ where $L = L_x = L_y$ [15]. The mirrors in the arms act as "freely falling" test masses [15]. To add the hardware injection signal to the data we physically displace the detectors' test masses in a way that mimics a gravitational-wave signal. In Initial LIGO, the test masses were displaced using electromagnetic actuators mounted on the the optic itself, however, these actuators are no longer mounted to the test masses due to noise. In aLIGO's first observing run, hardware injections were realized with two different actuation methods: electrostatic drive systems [16] and photon radiation pressure actuators referred to as "photon calibrators" [17]. The photon calibrators are currently the only actuator used to perform hardware injections since their actuation range available for hardware injections is larger.

During aLIGO's first observing run, astrophysical waveforms were injected using both actuation methods to test the detection and parameter estimation analyses. aLIGO is sensitive to a wide variety of astrophysical sources of gravitational waves including: binary black hole and/or neutron star mergers [18, 19], the stochastic gravitational-wave background [20], and isolated pulsars [21]. Hardware injections for each of these astrophysical sources were performed. In addition, series of sine-Gaussians were injected across the aLIGO frequency range to check for cross-couplings to the detectors' output channel.

This papers describes how we inject signals into the aLIGO detectors with the photon calibrators in Section II. Section III describes the results from analyses that used hardware injections in aLIGO's first observing run. This includes the recovery of binary black hole merger signals in Section III A and III B, the stochastic gravitational-wave hardware injection in Section III C, and a population of isolated pulsars in Section III D. A description of the detector characterization analysis to check for cross-couplings to the detectors' output channel is described in Section III E. Finally, Section IV summarizes the hardware injections and results from aLIGO's first observing run.

II. HARDWARE INJECTION PROCEDURE

Each astrophysical source has a different physical signal, and hence different technical requirements for the hardware injection system. In aLIGO's frequency range, compact binary mergers can last a fraction of a second to minutes depending on the component masses. We begin our hardware injection waveforms at 15 Hz, and as the two component masses inspiral closer together they sweep upward in frequency [6]. The merger's termination frequency and waveform length is determined by the masses of the two objects. For example, GW150914 terminates at 250 Hz [6], whereas the inspiral-only portion of a binary neutron star waveform with both component masses equal to 1.4 $M_\odot$ terminates at 1527 Hz. Isolated pulsars emit continuous gravitational waves at a particular frequency that is Doppler modulated by Earth's motion and the gravitational-wave frequency slowly evolves as the pulsar spins down [21]. The stochastic background is the superposition of many events that combine to create a low-level signal [20]. Non-astrophysically motivated injections include a succession of sine-Gaussians of short duration (< 1 s) used to search for couplings with the detector output channel.

The difference in the time duration of the sources requires separate controls, so we categorize hardware injections into two classes: "transient injections" that are localized in time, and "continuous-wave injections" that are active throughout the duration of the observing run. Examples of transient injections include binary black hole and/or neutron star mergers, sine-Gaussians, and stochastic background signals; we increase the amplitude of the stochastic background waveform in order to limit it to a short segment of data. Continuous-wave injections are a population of isolated pulsars. Separate automation processes control transient and continuous-wave injections. Fig. 1 shows a schematic of the two pathways that generate and transmit gravitational-wave strain time series to the photon calibrator. In this section we work through Fig. 1, beginning at the top-left and working clockwise, in order to describe the processes that control the transient and continuous-wave injections.

We generate the simulated gravitational waveforms for transient injection signals prior to injection. The system for managing the automated processes of the aLIGO detector subsystems is Guardian [22]. Guardian manages the transient hardware injections, it reads the next scheduled injection's time series and transmits the data to the digital control system of the detector at the scheduled

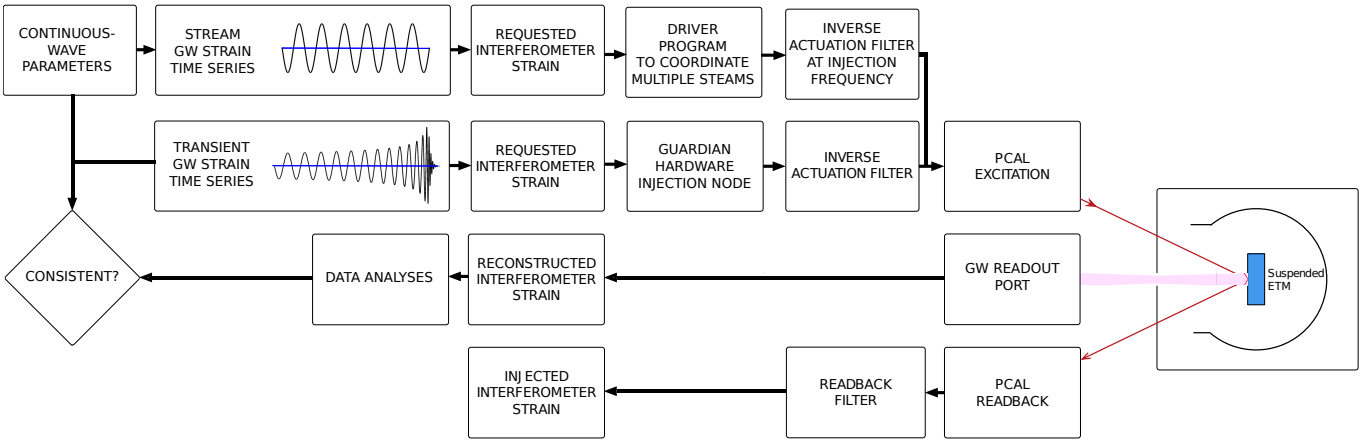

FIG. 1: Schematic diagram of the aLIGO hardware injection system. Time series for transient and continuous-wave injections are generated and sent to the photon calibrator (PCAL). The signal modulates the laser power of the photon calibrator to displace the end test mass (ETM) in a way that mimics a gravitational wave (GW) passing through the detector. The gravitational-wave strain of the detector is analyzed and checked for consistency. A photodiode monitors the reflected light from the test mass to measure the injected signal.

time.

Continuous-wave injections are generated in real-time. A streaming time series of simulated gravitational waves from a population of isolated pulsars, described by astrophysical parameters, including the strain amplitude, sky location, and initial frequency, is transmitted to the digital controls system of the detector. A driver program coordinates the simultaneous generation and buffering of multiple streams of signals representing spinning neutron stars [23].

The transient and continuous-wave signals in the digital controls system of the detector are sent to an actuator to reconstruct the gravitational-wave strain time series in the detectors' output channel. In aLIGO's first observing run, we used the electrostatic drive systems [16] and photon calibrators [17] as actuators for hardware injections. Each actuator has its own actuation pathway in the controls system; however, in Fig. 1 we show only the photon calibrators' pathway.

Hardware injections are carried out by actuating one of the end test masses (ETM) of the interferometer and thus inducing differential interferometer strain variations that simulate the response to an incident gravitational wave. The differential arm length degree of freedom of the interferometer is continuously maintained by a feedback control loop that actuates the longitudinal position of one of the ETM [10]. This feedback control loop suppresses the ETM displacement from noise sources. However, the servo does not suppress the ETM displacement that simulates the injected waveform, since there is a correction for the action of the servo when the strain is injected.

The actuators for the servo that maintains the differential arm length degree of freedom are electrostatic drive systems that apply forces via fringing field gradients from electrodes patterned onto a reaction mass separated by a few millimeters from the back surface of the ETM [16]. The electrostatic drive systems replaced the electromagnetic actuators mounted on the ETM in Initial LIGO. They were used at the beginning of aLIGO's first observing run for injecting simulated signals, including the waveforms for the GW150914 and stochastic background hardware injection analyses. However, the actuation range available for hardware injections is restricted because they are part of the differential arm length servo which consumes a significant fraction of their total actuation range in maintaining stable servo operation. In order to inject a larger parameter space of waveforms, for example binary black hole and/or neutron star mergers at closer distances, we transitioned to a photon calibrators for hardware injections.

We currently use a photon calibration system to simulate the displacement of the ETM from a gravitational-wave signal, this is depicted on the right of Fig. 1. A photon calibrator system uses an auxiliary, power-modulated laser with two beams impinging on the ETM located at the end of the x-arm of the interferometer. The photon calibrator on the other arm, the y-arm, is used for calibrating the detector output [17]. The two beams are diametrically opposed on the surface of the ETM, balanced in power, and positioned to minimize unintended torques and deformations of the surface which could cause errors in the expected displacement.

The aLIGO photon calibrators employ a feedback control system referred to as the "optical follower servo" [17]. This servo, with a bandwidth of $\sim$100 kHz, facilitates simulated signal injection via ETM actuation. This ensures that the laser output power modulation closely follows the analog voltage waveform injected at the servo input.

Digital infinite impulse response (IIR) compensation filters, called the "inverse actuation filters," convert the

requested interferometer strain signal (a digital signal) into an estimate of the photon calibrator optical follower servo input signal (an analog signal) required to achieve the desired length actuation. There is an analogous set of filters for the electrostatic drive system; however, we focus on the photon calibrators here. These filters are designed to compensate for several factors. There is compensation for: (i) the force-to-length transfer function of the suspended ETM, (ii) the signal conditioning electronics that includes a digital anti-imaging filter, the digital to analog converter gain, and an analog anti-imaging filter, and (iii) the optical follower servo transfer function. The digital IIR filters allowed by the aLIGO control system must be causal. Therefore they have known, but uncompensated, delays that we take into account during injection recovery.

The digital signals from the transient and continuous-wave injection pathways are passed through the inverse actuation filters, summed, and sent to the photon calibrator; see Fig. 1. Sporadic, unintended interruptions occurred in the Hanford injection system during aLIGO's first observing run, in which the buffering failed to keep up with real-time injection. The cause was not tracked down because of the unpredictable timing of the interruptions, but the drop-outs may be related to periods of high traffic on the controls system computer network. The sudden termination introduces a step function to the inverse actuation filters that has a large response at high frequencies. In the future, the effect of these dropouts, should they recur, will be mitigated by the use of point-by-point, Fourier-domain inverse actuation functions, using a separate, constant coefficient for each of the injected isolated pulsars, all of which are extremely narrowband. This is shown in the continuous-wave injection pathway in Fig. 1. Transient injections were not affected. Guardian sets the gain after the inverse actuation filters to zero while there is no active transient injection so unintended signals do not propagate into the detector data.

The strain actually injected into the interferometer is determined using the photon calibrator read-back signal generated by a power sensor that monitors the laser light reflected from the ETM, as shown at the bottom of Fig. 1. The output of this sensor is converted to injected interferometer strain using the read-back filter that compensates for the force-to-length transfer function as well as digital and analog filters in the signal read-back pathway. In the case of hardware injections, however, the excitation channel is calibrated by taking a transfer function measurement between the excitation channel and the read-back photodetectors. This transfer function is then incorporated within the inverse actuation filters. This provides a calibration accuracy on the order of a few percent, sufficient for the hardware injection analysis. For better calibration, however, we can compare the recovered signal and the injected signal as measured by the read-back photodetector.

There are some limitations to the photon calibrator system. First, the photon calibrator has a limited actuation strength, Fig. 2 shows the maximal displacement of the ETM using the photon calibrator system. The aLIGO photon calibrator can provide up to ∼1 W of peak power, but the force-to-length response of the ETM transfer function scales as the inverse-square of frequency [24]. Thus, the photon calibrator is limited in the amount of induced ETM displacement, especially at higher frequencies. Second, signal fidelity above ∼1 kHz is limited due to the shape of the anti-imaging filters and the desire to roll off the compensation filters close to the Nyquist frequency such that the compensation filters are not unstable. Nonetheless, the photon calibrator is able to provide precise, calibrated displacements of the ETM in response to many astrophysical waveforms.

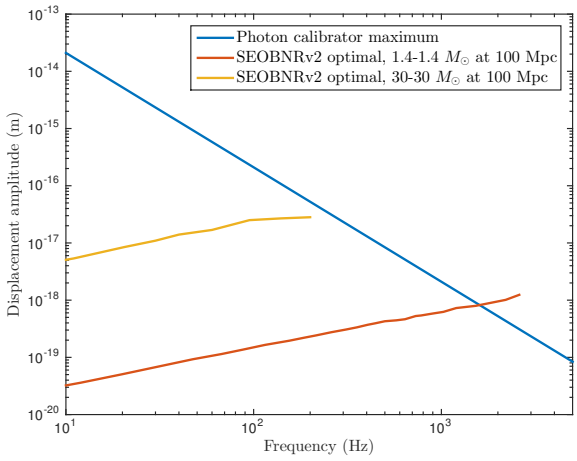

FIG. 2: The maximum displacement of an ETM using the photon calibrator (blue). The maximum displacement of the ETM required for two compact binary waveforms that contain an inspiral, merger, and ringdown are shown for reference; a 30-30 $M_\odot$ binary at 100 Mpc (yellow) and 1.4-1.4 $M_\odot$ binary at 100 Mpc (red) were generated using the SEOBNRv2 approximant [25]. Note that the required displacement for the 1.4-1.4 $M_\odot$ binary exceeds the maximal photon calibrator displacement at high frequencies, however, an inspiral-only waveform for a 1.4-1.4 $M_\odot$ binary at 100 Mpc would terminate at 1527 Hz.

III. RESULTS

In this section we describe results from hardware injection analyses in aLIGO's first observing run. Hardware injections were used as: (i) an end-to-end test of searches and parameter estimation analyses, (ii) an additional check of the calibration, and (iii) a method to check for cross-couplings to the detectors' output channels. Binary black hole waveforms with parameters similar to GW150914 and GW151225 were used to test modeled and unmodeled analyses described in Section III A and III B. A simulated stochastic gravitational-wave signal was recovered with the analysis described in Sec-

tion III C. The population of isolated pulsars analysis in Section III D provided an additional check of the calibration; they were used to verify the overall sign of the detectors' calibration and to measure the time delay between the hardware injection excitation channel and the detectors' output channels. These astrophysical signals were injected coherently into the Hanford (H1) and Livingston (L1) detectors. Section III E describes the study that injects a series of sine-Gaussians across the aLIGO frequency range to check for cross-couplings to the detectors' output.

A. Compact Binary Coalescence

aLIGO observed gravitational waves from binary black hole mergers in its first observing run [6, 7]. After a detection, similar gravitational-wave signals were injected into the interferometer data and recovered by search and parameter estimation analyses as a high-level sanity check. Compact binary coalescence searches use matched filtering to correlate aLIGO data with a bank of gravitational-wave templates. Here we consider hardware injections analyzed by the PyCBC search for gravitational waves described in [26]. Parameter estimation analyses were used to analyze the hardware injections and check for consistency with GW150914 and GW151226. We ran the same algorithm used to characterize the detected events [27, 28]. We show the recovery of hardware injections with parameters taken from posterior distributions of parameter estimation results for GW150914 [28] and GW151226 [7, 19].

For each gravitational-wave detection we injected ten waveforms coherently into the two detectors. The GW150914 hardware injections were generated with the SEOBNRv2 waveform approximant and included only component spins aligned with the angular momentum of the binary [25]. These signals were injected October 2 to October 6, 2015. The GW151226 hardware injections were generated with the precessing waveform approximant IMRPhenomPv2 [29, 30] and injected on January 11, 2016.

PyCBC reports a detection statistic $\hat{\rho}$ [31] that combines information about the matched-filter signal-to-noise ratio ρ and the degree to which it is consistent with a compact binary signal χ^2_r [12]. We checked the search's matched-filter output, Fig 3 shows the reported ρ versus the expected ρ calculated using software injections for 19 of the 20 hardware injections. One of the GW150914 hardware injection had a matched-filter signal-to-noise ratio < 5.5 in Livingston. In order to manage computational considerations, the analysis requires a single-detector signal-to-noise ratio of at least 5.5. Thus, this injection was not "detected." A signal-to-noise ratio < 5.5 for this injection, with an expected signal-to-noise ratio of 6, is consistent with the variation of the matched-filter output in Gaussian noise [32].

The expected signal-to-noise ratio was calculated using software injections, in which signals are added to the data without any physical actuation. While hardware injections are an important end-to-end test, software injections are useful because a large number can be performed without perturbing the detector or significantly reducing the duty cycle of the detectors. Fig. 3 shows the software injections to be consistent with the recovery of signals that propagate through the detectors, therefore we can generate large populations of software injections that are used in other studies to evaluate the search efficiency [26], detections [33], and binary merger rates [18, 19].

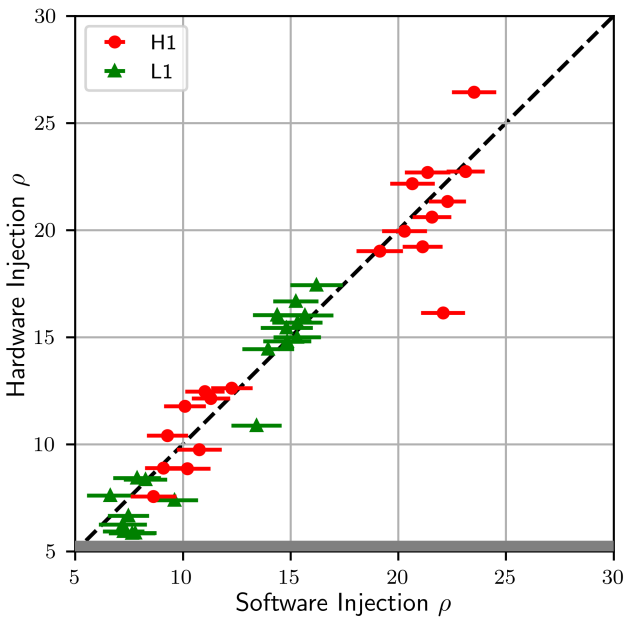

FIG. 3: A comparison of the signal-to-noise ratio ρ from software injections and the recovered signal-to-noise ratio of the hardware injection. The software injection ρ is the mean and 1σ error from the recovery of 50 software injections filtered with the injected waveform near the time of the injection. The threshold on ρ is indicated by the gray region.

In Fig. 3 there is one GW150914 hardware injection that was recovered with a signal-to-noise ratio of 16.1 and 10.9 in Hanford and Livingston respectively; however, the injection had an expected signal-to-noise ratio of 22.1 and 13.4. This injection was recovered with a lower signal-to-noise ratio because the search clusters nearby maxima in the signal-to-noise time series [26], and a loud transient noise artifact was present in the Livingston data shortly after the hardware injection. Fig. 4 shows the Livingston signal-to-noise ratio time series for the injected binary black hole waveform. The χ^2_r statistic [12] downweights the detection statistic $\hat{\rho}$ [26] of the noise transient. Lower mass templates in the bank of waveforms were less sensitive to the noise transient and therefore the search was able to recover the injection with a lower signal-to-noise ratio.

We compared the false-alarm rate [26] of the hardware injections and a large population of software injections.

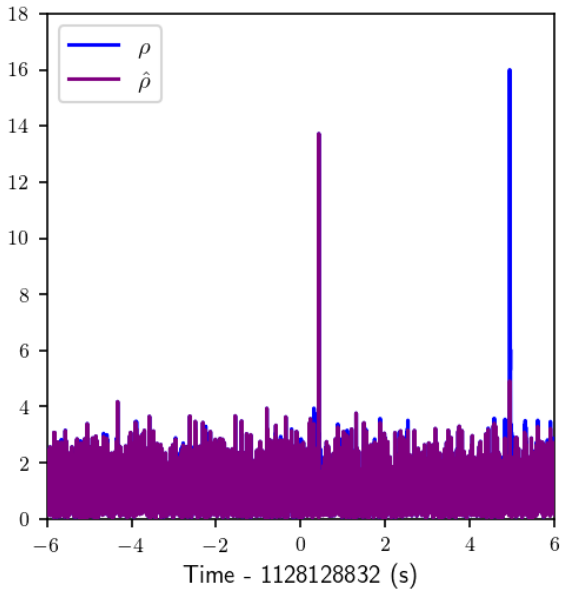

FIG. 4: The Livingston signal-to-noise ratio ρ and detection statistic $\hat{\rho}$ versus time. The hardware injection is centered near 0 s. A noise transient is in the data at ∼5 s with a higher signal-to-noise ratio. The noise transient has a lower $\hat{\rho}$ than the hardware injection.

Fig. 5 shows the χ^2_r statistic [12] versus ρ for maxima in the signal-to-noise ratio time series. Astrophysical events are indicated with stars. Hardware injections are indicated with squares. Software injections are denoted by crosses. The software injections in Fig. 5 are generated from a population of aligned-spin binaries with source-frame component masses between 2 to 98 $M_\odot$ using the SEOBNRv2 waveform approximant [25]. The population of signals is randomly distributed in sky location, orientation, distance, and time. The injection times are within the 39 day period around GW150914 reported in [33].

We see a separation of the software injections with high significance (false-alarm rate $< 1/100\,\mathrm{yr}^{-1}$) and background distributions. All ten GW150914 hardware injections are recovered with high significance. Although the GW151226 Livingston hardware injections are not visibly distinguishable from the background distribution in Fig. 5, seven hardware injections have a highly significant false-alarm rate ($< 1/100\,\mathrm{yr}^{-1}$) when we combine data from both detectors. Two hardware injections were recovered with $1/10\,\mathrm{yr}^{-1} >$ false-alarm rate $> 1/100\,\mathrm{yr}^{-1}$, a significance comparable to the gravitational-wave candidate LVT151012 ($1/2\,\mathrm{yr}^{-1}$) reported in aLIGO's first observing run [6].

If a detection candidate is a true gravitational wave, we should be able to reproduce the morphology of the posterior distributions using the hardware injections. Conversely any significant differences have the potential to highlight discrepancies between the observation and our waveform models. Here we focus on two parameters: chirp mass and sky location.

The chirp mass $\mathcal{M}$ is defined as

$$\mathcal{M} = \frac{(m_1 m_2)^{3/5}}{(m_1 + m_2)^{1/5}}. \quad (1)$$

Here, m_1 and m_2 are the binary's component masses. The chirp mass is typically the best estimated parameter of a compact binary coalescence signal, since it dominates the phase evolution during inspiral. In Fig. 7 we show for all the GW151226 hardware injections the posterior distributions of the chirp mass minus the respective injected values, using the precessing waveform approximant IMRPhenomPv2 [29, 30]. Most posteriors have comparable width, hardware injections with low signal-to-noise ratio have broader distributions and in one case shows bimodality. The width of the 90% confidence interval for the detector-frame chirp mass for GW151226 is $\sim 0.12\ M_\odot$ [19], which is comparable to that found with the hardware injections.

Sky maps of GW150914 and GW151226 were shared with electromagnetic observatories [34, 35] and are show in [19, 36]. In Fig. 6, we show a reconstructed Earth-bound coordinate sky map for GW151226 along with maps for two hardware injections. One of the two hardware injections (at GPS time 1136588345) has low signal-to-noise ratio and thus spans a larger sky area, although still along the same triangulation ring. The other injection (at GPS time 136592746) is instead representative of the typical map: all other maps look similar to this and are not shown to avoid overcrowding.

A previous study used the parameter estimation method described above to validate another strategy used to interpret GW150914, by directly comparing data to simulations of Einstein's equations [37]. In that study the parameter estimates for GW150914 derived from IMRPhenomPv2 and numerical relativity agreed [37]. This study was repeated comparing hardware injections to numerical relativity, and found posterior distributions in mass and spin were consistent with the IMRPhenomPv2 analysis.

B. Burst

There are astrophysical sources of gravitational waves that have poorly modeled or unknown waveforms, such as core-collapse supernovae [38]. In order to search for a wide range of unmodeled astrophysical sources, analyses look for short-duration, transient gravitational-wave events referred to as "bursts" [39]. Here, we look at injection recoveries using: Coherent WaveBurst [40], BayesWave [41], and LALInferenceBurst [42, 43]. These analyses produce reconstructed waveforms with minimal assumptions about the waveform morphology. We compare these reconstructions to the injected waveforms of hardware injections.

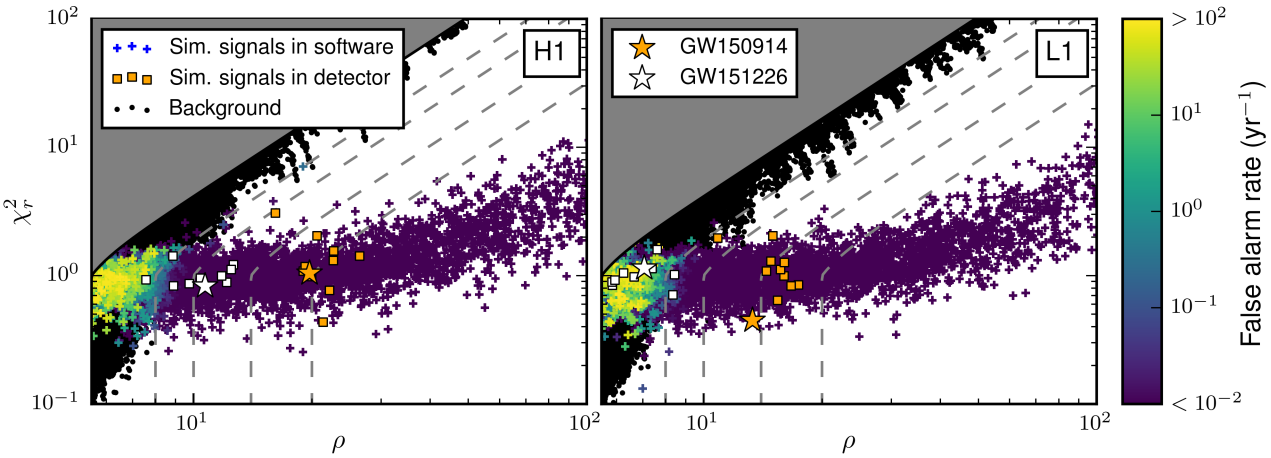

FIG. 5: PyCBC χ^2_r statistic versus matched-filter signal-to-noise ratio ρ for each detector. Software injections are represented as crosses that are colored by false-alarm rate. The gravitational-wave events GW150914 and GW151226 are shown as stars. Hardware injections for GW150914 and GW151226 are represented as boxes. Background distributions (black dots) are plotted; there was a threshold applied indicated by the gray region. Lines of constant detection statistic $\hat{\rho}$ are shown (gray dashed lines); plotted are $\hat{\rho} = \{8, 10, 14, 20\}$.

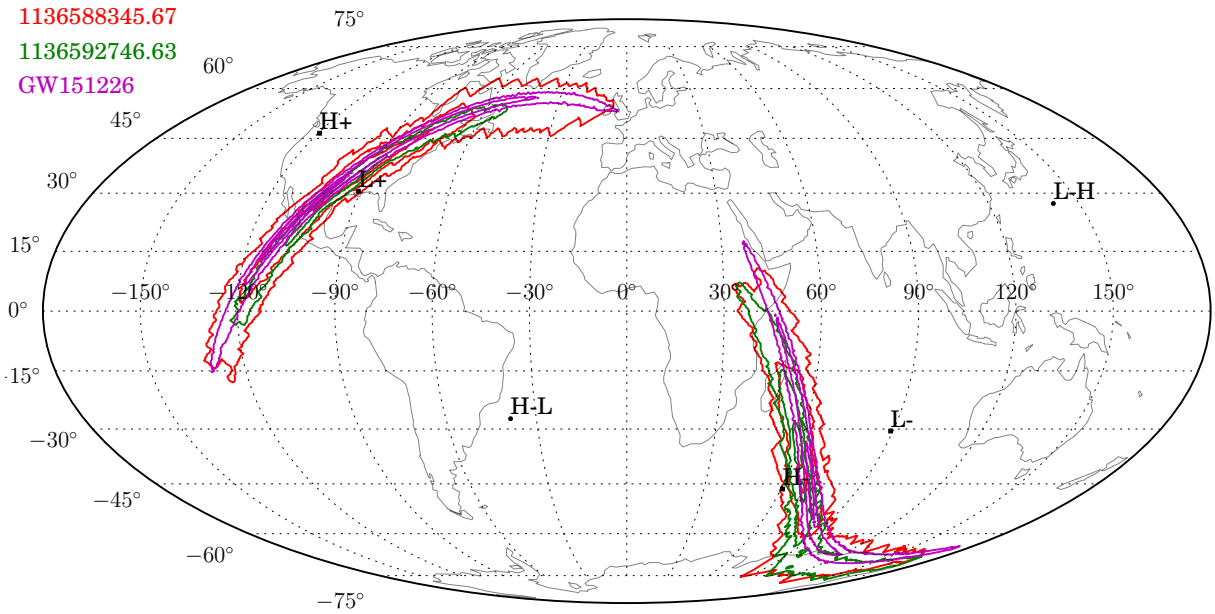

FIG. 6: The 90% confidence interval skymaps for two hardware injection (red and green) and GW151226 (magenta). The skymaps are show in Earth-bound coordinates. The two hardware injections are chosen to be representative of an average event (green) and a sub-threshold event (red). We notice how all sky maps have support on the same ring of equal time delay between the two aLIGO detectors.

In addition to the ten GW150914 hardware injections described in Section III A, there were 24 waveforms with physical parameters similar to GW150914 injected. Eight were non-spinning waveforms with equal component masses and a total mass of 76 $M_\odot$; sixteen were aligned-spin with total masses from $[70, 80]$ $M_\odot$ and mass ratios from 1 to 5. Mass ratio is defined as m_1/m_2 where $m_1 > m_2$. The waveforms were generated with the SEOBNRv2 approximant [25].

Since burst searches do not use gravitational-wave templates, they are less sensitive to compact merger signals than modeled searches [44]. The burst searches did not

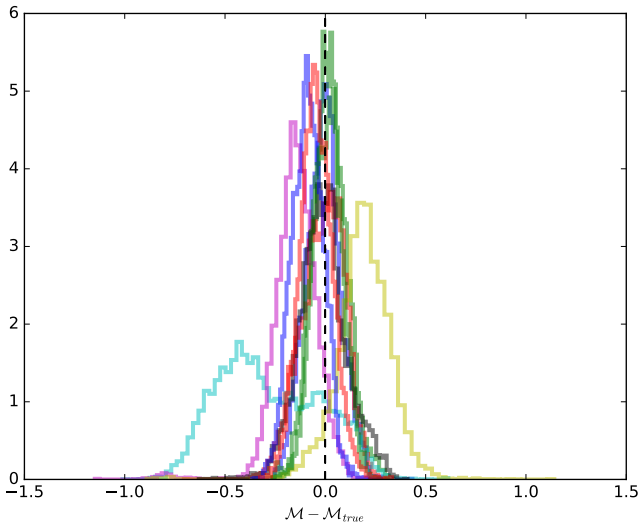

FIG. 7: Posterior distributions for the chirp mass of the GW151226 hardware injections. The true value has been removed to center all distributions around zero. Hardware injections with very low signal-to-noise ratio show large width and in one case bimodality. The bimodal distribution comes from the injection at GPS time 1136588345 which is also shown in Fig. 6.

recover GW151226, and recovered only a single hardware injection performed to validate that detection. The recovery of GW151226 hardware injections using the burst analyses are not discussed in this paper.

Coherent WaveBurst identifies coherent events in spectrographic data from the aLIGO detectors constructed using a wavelet representation. It then reconstructs the gravitational waveform using a likelihood analysis [40]. For signals consistent with compact binary coalescences, it also estimates the system's chirp mass based on the time-frequency evolution of the signal [45]. The low-latency Coherent WaveBurst search recovered 28 of the 34 total injections. In Fig. 8 we show the recovered versus injected excess power signal-to-noise ratio and chirp mass. Note that the excess power signal-to-noise ratio [40] is distinct from the matched-filter signal-to-noise ratio ρ.

BayesWave uses a sum of sine-Gaussian wavelets to model the gravitational-wave signal [41]. The reconstruction assumes an elliptically polarized gravitational wave, but no other constraints are imposed [41]. BayesWave investigated the 28 GW150914 hardware injections recovered by Coherent WaveBurst. Previous studies with software injections show that the recovered waveforms produced by BayesWave accurately match injected signals [39]. To measure the overlap between injected and recovered waveforms, we use the network match

$$\text{Match} = \frac{(h_{\rm inj}|h_{\rm rec})}{\sqrt{(h_{\rm inj}|h_{\rm inj}) \times (h_{\rm rec}|h_{\rm rec})}} \tag{2}$$

where $h_{\rm inj}$ is the injected waveform, $h_{\rm rec}$ is the recovered waveform, and $(a|b)$ is the noise-weighted inner product summed over all interferometers [41]. The average network match between the injected and reconstructed waveforms is 94%. The 94% match is consistent with the average match found using software injections [39]. An example of a reconstructed waveform is shown in Fig. 9.

Coherent WaveBurst, BayesWave, and LALInferenceBurst provide sky localization estimates as the signal is reconstructed. Fig. 10 demonstrates sky maps for one of the GW150914 hardware injections and GW150914 itself [28]. We see similar support in Earth-bound coordinates, and nearly identical structures around the triangulation rings. The right-hand panels of Fig. 10 highlight this with the posterior distributions for the time delay between the two detectors.

C. Stochastic

A stochastic gravitational-wave background is expected to arise from the superposition of many events, each of which are too weak to resolve, but which combine to create a low-level signal [20]. By cross correlating data from two or more detectors, it is possible to detect low-level correlations hidden beneath the detectors' noise [46]. The stochastic background from unresolved binary black holes is a particularly promising source, potentially within reach of advanced detectors [47]. On October 23, 2015, a stochastic gravitational-wave background signal was simultaneously injected into both detectors. The 600 s-long signal corresponded to an isotropic Gaussian background.

The strength of a stochastic gravitational-wave signal is parameterized by the fractional contribution of the energy density in gravitational waves to close the Universe [46]:

$$\Omega_{\rm GW}(f) = \frac{1}{\rho_c}\frac{{\rm d}\rho_{\rm GW}}{{\rm d}\ln f}. \tag{3}$$

Here, ρ_c is the critical energy density of the Universe, f is frequency, and $d\rho_{\rm GW}$ is the energy density between f and $f + df$. The injected signals were chosen such that $\Omega_{\rm GW}(f) = 8.7\times10^{-5}$. This corresponds to a strain power spectral density of

$$\begin{aligned} S_h(f) &= \frac{3H_0^2}{10\pi^2}\frac{\Omega_{\rm GW}(f)}{f^3} \\ &= \left(2.9\times10^{-23}\,{\rm Hz}^{-1/2}\right)^2\left(\frac{25\,{\rm Hz}}{f}\right)^3 \end{aligned} \tag{4}$$

where H_0 is the Hubble constant.

We carried out a cross-correlation search following the standard procedure [48]. The data was split into 50%-overlapping, 60 s intervals, and utilizing coarse-grained 0.25 Hz-wide frequency bins, we recovered an $\Omega_{\rm GW}(f)$ of $(8.8\pm0.6)\times10^{-5}$, consistent with the injected value. The recovered signal is shown in Fig. 11. The y-axis shows

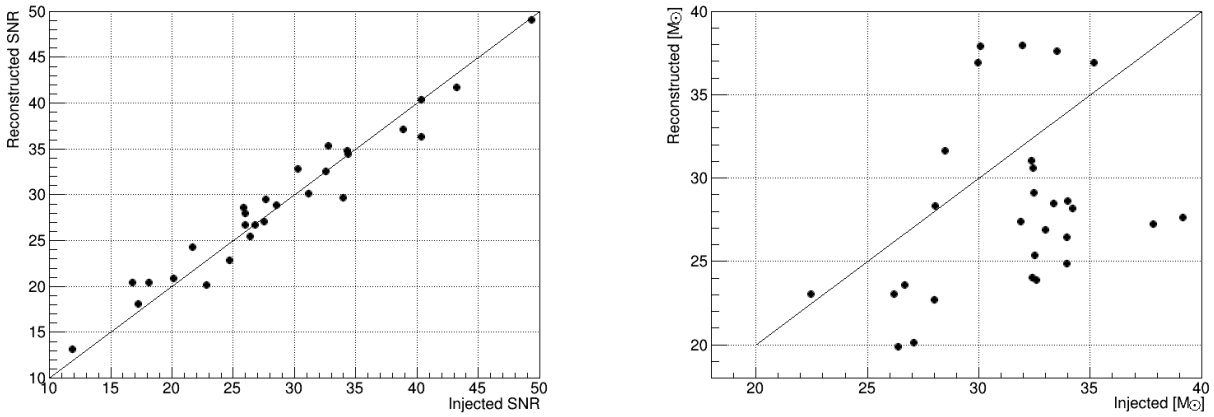

FIG. 8: The 28 recovered hardware injections by the low-latency Coherent WaveBurst search. *Left:* Recovered excess power signal-to-noise ratio (Reconstructed SNR) versus injected excess power signal-to-noise ratio (Injected SNR). *Right:* Recovered chirp mass (Reconstructed) versus injected chirp mass (Injected).

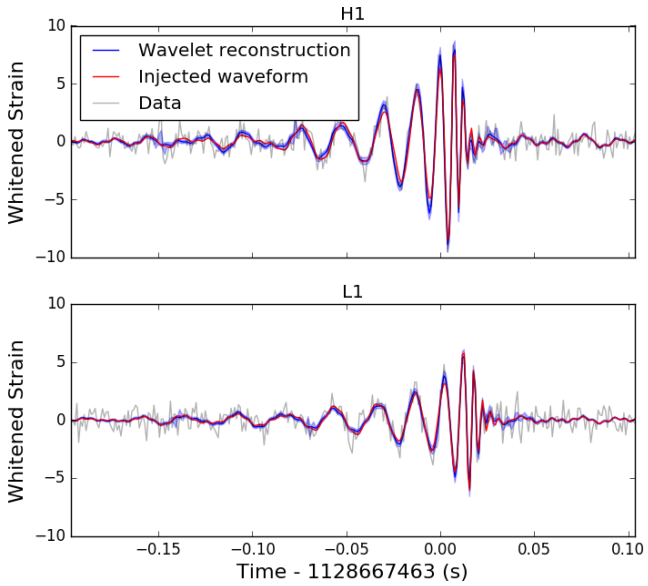

FIG. 9: BayesWave median reconstruction and 90% credible interval (blue) and the injected waveform (red), time is shown on the x-axis and whitened strain on the y-axis. The data has been whitened using the estimated noise curve from the time of the injection. The network match for this waveform is 98%.

the recovered signal as a function of the time lag between the detectors. A peak at zero, and the absence of structure at other times, shows that the signal is recovered as expected.

D. Continuous Wave

The recovery of hardware injections is used by continuous-wave searches as an end-to-end validation of the analyses in the presence of instrumental artifacts and imperfect instrument calibration. Coherent searches for known pulsars are sensitive to deviations from the injected signal since a small bandwidth around the gravitational-wave frequency is integrated for months or years [21]. These searches have the capability of monitoring the self-consistency of the interferometer calibration and, in particular, the long-term stability of absolute phase recovery. Continuous-wave searches can be implemented using radiometer [49, 50] or Bayesian methods [21]. Here, we consider a coherent search based on Bayesian recovery of signal parameters [21] to validate the fidelity of hardware injections. This analysis can be used to cross-check elements of the instrument calibration, including proper coherence of data from interferometers separated by thousands of kilometers, which are sensitive to timing errors.

Fig. 12 shows the posterior for strain amplitude h_0 for a pulsar, which has a signal frequency near 108.9 Hz and a nearly linear polarization. The signal is recovered with an amplitude consistent with the intended strength, within calibration and actuation uncertainties. Similarly, Fig. 12 also shows the recovered phase constant for this injection. In the analysis there is no compensation for the time delay between the hardware injection excitation channel and the detector output channel. Consistency with the expectation for the phase constant is observed, given an uncompensated time delay.

During aLIGO's first observing run, there were 15 isolated pulsars streaming in real-time with frequencies ranging from $12 - 1991$ Hz. Figs. 13 and 14 show a summary of the agreement between recovered and intended amplitude and phase for the 14 injections with sufficient signal-to-noise ratio to permit recovery. Instrumental noise at the lowest-frequency injection (12 Hz) proved too large to permit signal recovery. There is evidence of a constant uncompensated time delay of about

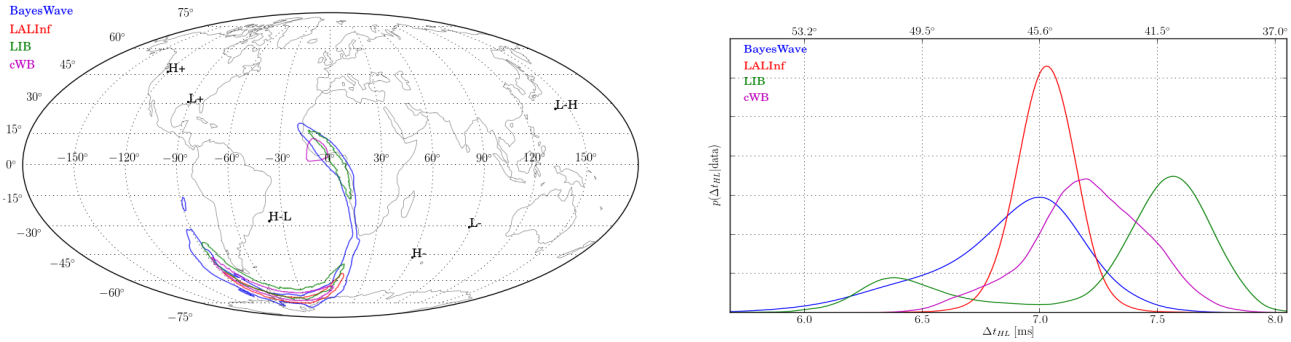

(a) Hardware injection on October 2, 2015, at 01:16:43 GMT

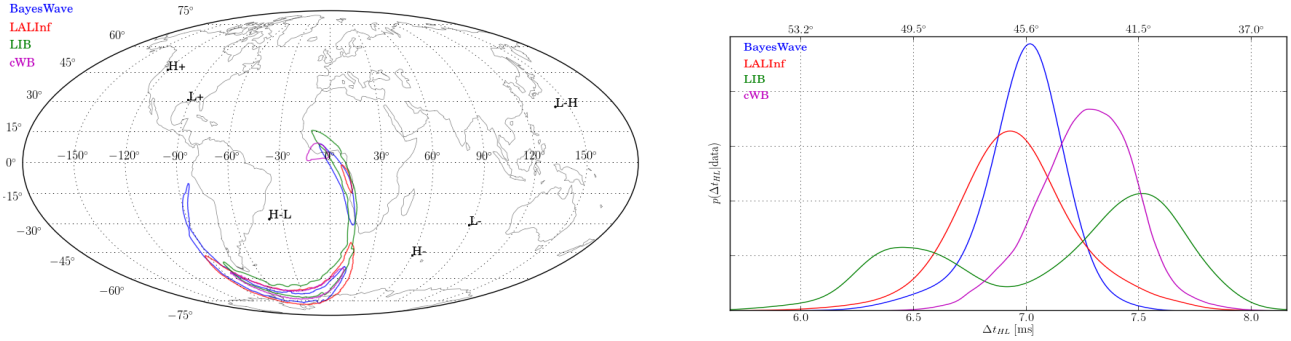

(b) GW150914

FIG. 10: Sky localizations estimates from burst analyses: BayesWave, Coherent WaveBurst (cWB), and LALInferenceBurst (LIB). We include the parameter estimation analysis from Section III A (LALInf) for comparison [28]. *Left:* We show the localization maps in Earth-bound coordinates for a GW150914 hardware injection and GW150914 itself. *Right:* To highlight the similar positions relative to the detectors the marginal distributions for the time delay between the two detectors is shown.

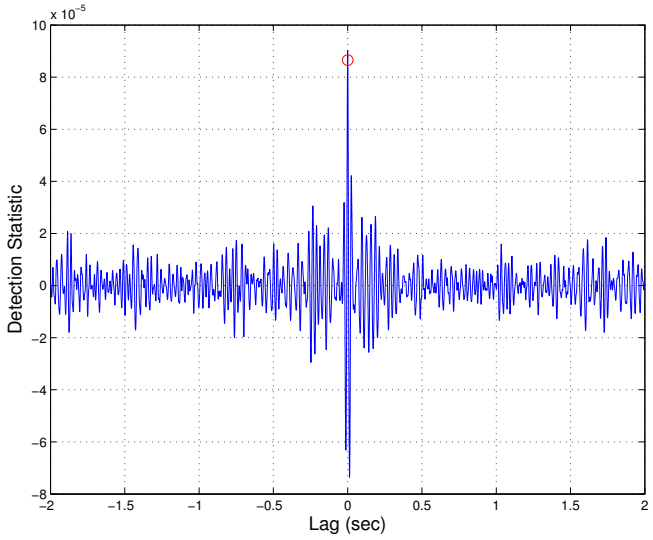

FIG. 11: Recovered stochastic signal as a function of lag time between detectors (blue). The injected signal is represented with a red circle. The peak of the recovered signal intersects with the injection at zero lag, indicating a successful recovery.

150 μs in the time-domain actuation, which manifests as a phase delay increasing linearly with injection frequency in Fig. 14. In the future, a compensating timing advance will be included in the inverse actuation filter, and the pulsars' amplitudes will be increased for more precise and rapid validation of the hardware injection signal.

The overall sign of the calibration is important in order to detect and estimate the parameters of astrophysical signals correctly. An incorrect sign on the calibration would invert the signal in one detector and the parameter estimates would be incorrect. The continuous-wave injections were used as an additional check on the sign of the calibration between the aLIGO detectors, since an incorrect sign would lead to a relative phase offset between the two detectors in Fig. 14. We found the sign of the calibration to be correct.

E. Detector Characterization

Noise artifacts in aLIGO data adversely affect the output of gravitational-wave search analyses [8, 9]. In searches for transient gravitational waves, some periods of time are excluded from the analysis to remove periods of poor data quality and known transient noise. These are known as "data quality vetoes" [8, 9]. Removing periods of time with excess noise improves the performance of gravitational-wave searches [8, 9]. Some of these data quality vetoes are derived from information recorded in auxiliary channels. Auxiliary channels include instrumental channels that record degrees of freedom of the interferometer and its isolation systems as well as channels that monitor the environmental conditions around the instrument [51]. The environmental monitoring system includes seismic, acoustic, and electromagnetic data.

To avoid discarding true gravitational-wave signals, any auxiliary channels used for vetoes are first checked to ensure that they do not respond to gravitational-wave-like signals; i.e., changes in differential arm-length. This process is referred to as a "safety check," since a channel that has no sensitivity to gravitational waves is considered "safe" for use when constructing a veto. To test whether auxiliary channels respond to differential arm-length changes, three sets of 12 loud (matched-filter signal-to-noise ratios > 100) transient hardware injections were performed at both detectors, and the auxiliary channel data were examined both qualitatively and quantitatively for signs of coupling.

Spectrograms were manually inspected at the time of hardware injections. These signals were very strong and clear, with high signal-to-noise ratio, in channels that were expected to record differential displacement, e.g. interferometer differential sensing and actuation, and closely related degrees of freedom. No signs of coupling were found in thousands of other auxiliary channels, indicating that they may be used to construct vetoes. Thousands of time-frequency representations of auxiliary channels were also inspected at the times of GW150914 and GW151226 with the same outcome [8].

Loud hardware injections were used to statistically assess the coupling. An algorithm based on a transformation using sine-Gaussians [52] was used to identify and parameterize noise transients by their time, frequency, and signal-to-noise ratio. The time of noise transient is compared with the times of the loud hardware injections. For each channel, the number of noise transients that occurred within 100 ms of loud injections are counted and compared to the number that would be expected based on chance [53]. For any channel exhibiting a higher number of overlaps than expected by chance, the time-frequency behavior of the raw data is further investigated to see if there is a plausible connection. We find that only obviously related channels, such as those in the sensing and actuation chain for the differential length control loop, were sensitive to the loud hardware injections.

IV. CONCLUSIONS

This paper presents the aLIGO hardware injection system infrastructure for injecting signals into the interferometers and results from aLIGO's first observing run. Hardware injections were used for validating analyses after a gravitational-wave detection, an additional check of the calibration, and detector characterization.

After the detection of GW150914 and GW151226, sets of binary black hole merger waveforms with similar parameters were injected to validate the search and parameter estimation analyses. The recovered signals were checked for consistency with the injected waveforms, including signal-to-noise ratio, chirp mass, and sky position. Similarly, the stochastic background and

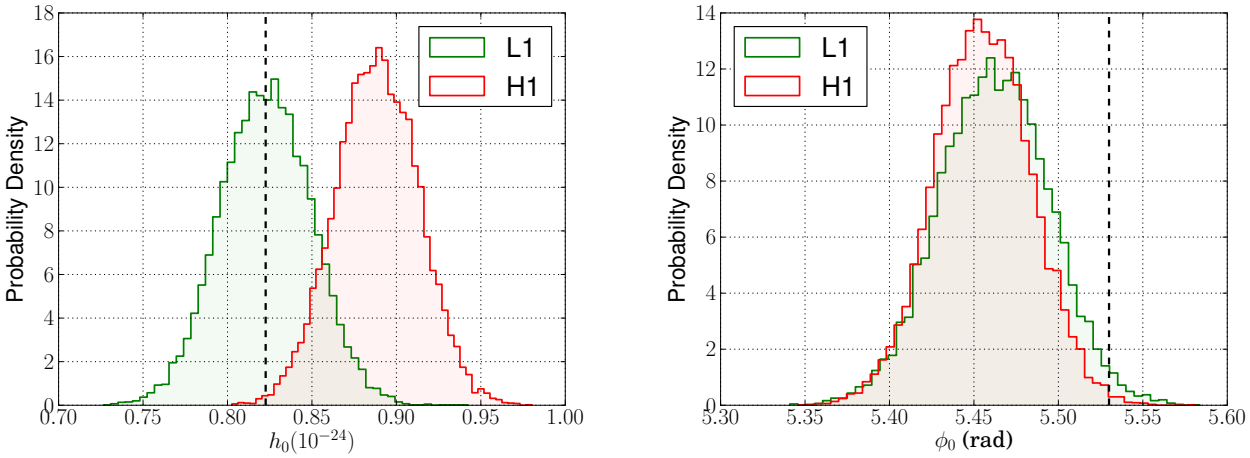

FIG. 12: Posterior probability density functions for the recovered strain amplitude and phase constant for the pulsar at 108.86 Hz. The dashed vertical line indicates the intended injection amplitude and phase in radians. The red and green curves indicate the separately recovered amplitudes and phases for the Hanford and Livingston interferometers, respectively. The apparent residual discrepancies in amplitude and phase fall within the uncertainties of the actuation system used for the injections.

continuous-wave searches used simulated waveforms as an end-to-end test.

In order to detect and estimate the parameters of astrophysical signals the calibration must be correct, and the continuous-wave injections provided an additional check of the calibration sign. They were also used to measure the time delay of the hardware injection pathway and checked that it was consistent with the predicted value from the calibration model.

Data quality vetoes are used to increase the performance of search analyses, and detector characterization hardware injections were used to identify channels in the control system that can be used to construct data quality vetoes. After each gravitational-wave detection, we carried out a study to check for cross-couplings with the detectors' output channel. Channels that contained a trace of the injected signal were excluded from data quality veto studies.

In the future, we plan to exclusively use the photon calibrators to inject simulated gravitational waves. Future work on the hardware injection system includes using point-by-point, Fourier-domain inverse actuation functions for each of the injected isolated pulsars to mitigate the effect of data dropouts. There are no plans to perform blind injections in future observing runs.

[1] J. Aasi et al. (LIGO Scientific), Class. Quantum Grav. **32**, 074001 (2015).
[2] F. Acernese et al. (VIRGO), Class. Quantum Grav. **32**, 024001 (2015).
[3] H. Grote (LIGO Scientific), Class. Quantum Grav. **27**, 084003 (2010).
[4] Y. Aso, Y. Michimura, K. Somiya, M. Ando, O. Miyakawa, T. Sekiguchi, D. Tatsumi, and H. Yamamoto (KAGRA), Phys. Rev. **D88**, 043007 (2013).
[5] B. Iyer et al., *LIGO-India Tech. Rep.* (2011), URL `https://dcc.ligo.org/LIGO-M1100296/public`.
[6] B. P. Abbott et al. (Virgo, LIGO Scientific), Phys. Rev. Lett. **116**, 061102 (2016).
[7] B. P. Abbott et al. (Virgo, LIGO Scientific), Phys. Rev. Lett. **116**, 241103 (2016).
[8] B. P. Abbott et al. (Virgo, LIGO Scientific), Class. Quantum Grav. **33**, 134001 (2016).
[9] J. Aasi et al. (VIRGO, LIGO Scientific), Class. Quantum Grav. **32**, 115012 (2015).
[10] B. P. Abbott et al. (LIGO Scientific) (2016), 1602.03845.
[11] E. Thrane, N. Christensen, R. M. S. Schofield, and A. Effler, Phys. Rev. **D90**, 023013 (2014).
[12] B. Allen, Phys. Rev. **D71**, 062001 (2005).
[13] J. Abadie et al. (VIRGO, LIGO), Phys. Rev. **D85**, 082002 (2012).
[14] J. Abadie et al. (VIRGO, LIGO), Phys. Rev. **D81**, 102001 (2010).
[15] B. P. Abbott et al. (Virgo, LIGO Scientific), Phys. Rev. Lett. **116**, 131103 (2016).
[16] L. Carbone et al., Class. Quantum Grav. **29**, 115005 (2012).
[17] S. Karki et al. (2016), 1608.05055.
[18] B. P. Abbott et al. (Virgo, LIGO Scientific) (2016), 1607.07456.
[19] B. P. Abbott et al. (Virgo, LIGO Scientific), *Binary Black Hole Mergers in the first Advanced LIGO Observing Run* (2016).
[20] M. Maggiore, Phys. Rept. **331**, 283 (2000).

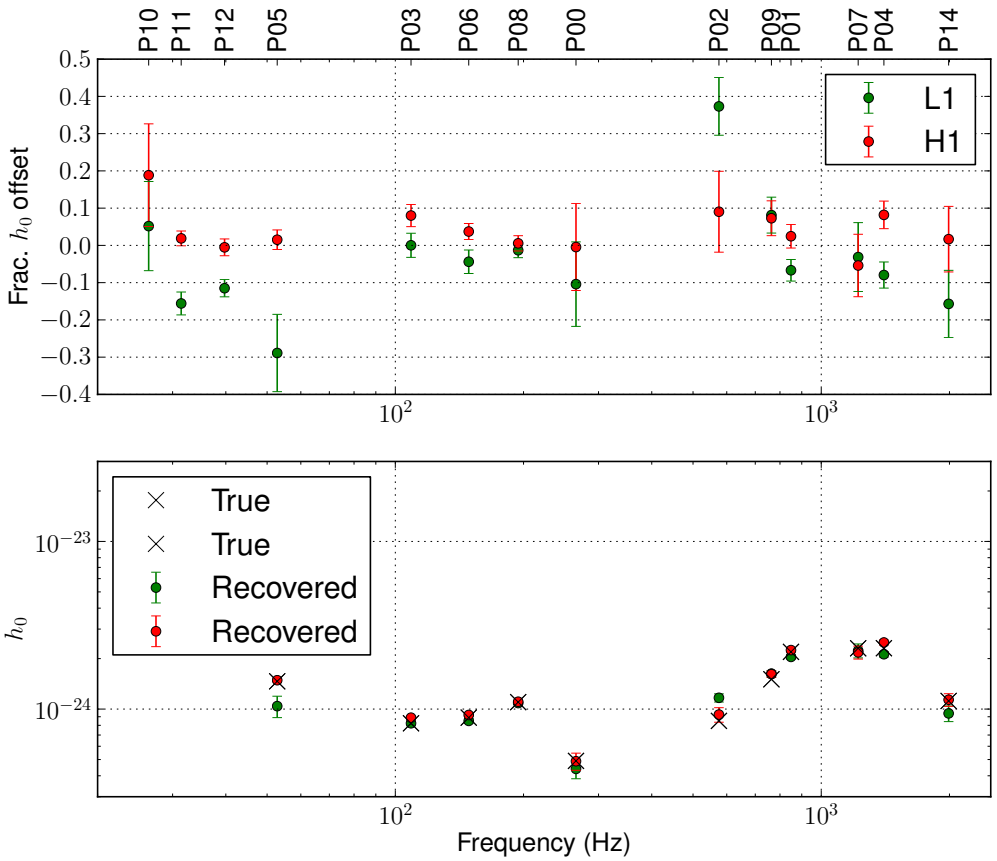

FIG. 13: Comparisons of recovered signal amplitudes for the Hanford and Livingston signals for the 14 recovered continuous-wave injections (P00-P14). *1st panel:* Fractional amplitude difference [(recovered minus injected)/injected]. *2nd panel:* Amplitude values (recovered and injected).

[21] J. Aasi et al. (LIGO Scientific), Astrophys. J. **785**, 119 (2014).

[22] J. Rollins, *Advanced LIGO Guardian Documentation* (2015), URL `https://dcc.ligo.org/LIGO-T1500292/public`.

[23] LSC Data Analysis Software Working Group, *LALSuite*, https://www.lsc-group.phys.uwm.edu/daswg/projects/lalsuite.html, URL `https://www.lsc-group.phys.uwm.edu/daswg/projects/lalsuite.html`.

[24] E. Goetz, P. Kalmus, S. Erickson, R. L. Savage, G. Gonzalez, K. Kawabe, M. Landry, S. Marka, B. O'Reilly, K. Riles, et al., Class. Quantum Grav. **26**, 245011 (2009).

[25] A. Taracchini, Y. Pan, A. Buonanno, E. Barausse, M. Boyle, T. Chu, G. Lovelace, H. P. Pfeiffer, and M. A. Scheel, Phys. Rev. **D86**, 024011 (2012).

[26] S. A. Usman et al., Class. Quantum Grav. **33**, 215004 (2016).

[27] J. Veitch et al., Phys. Rev. **D91**, 042003 (2015).

[28] B. P. Abbott et al. (Virgo, LIGO Scientific), Phys. Rev. Lett. **116**, 241102 (2016).

[29] P. Schmidt, F. Ohme, and M. Hannam, Phys. Rev. **D91**, 024043 (2015).

[30] M. Hannam, P. Schmidt, A. Bohè, L. Haegel, S. Husa, F. Ohme, G. Pratten, and M. Pürrer, Phys. Rev. Lett. **113**, 151101 (2014).

[31] S. Babak et al., Phys. Rev. **D87**, 024033 (2013).

[32] D. A. Brown, Ph.D. thesis, Wisconsin U., Milwaukee (2004), 0705.1514, URL `https://inspirehep.net/record/673638/files/arXiv:0705.1514.pdf`.

[33] B. P. Abbott et al. (Virgo, LIGO Scientific), Phys. Rev. **D93**, 122003 (2016).

[34] L. Singer et al. (2015), URL `http://gcn.gsfc.nasa.gov/other/GW150914.gcn3`.

[35] L. Singer et al. (2015), URL `http://gcn.gsfc.nasa.gov/other/GW151226.gcn3`.

[36] L. S. Collaboration and the Virgo Collaboration (2016).

[37] B. P. Abbott et al. (Virgo, LIGO Scientific), Phys. Rev. **D94**, 064035 (2016).

[38] C. L. Fryer and B. K. C. New, *Gravitational waves from gravitational collapse* (2011).

[39] B. P. Abbott et al. (Virgo, LIGO Scientific), Phys. Rev. **D93**, 122004 (2016), [Addendum: Phys. Rev. **D94**, 069903 (2016)].

[40] S. Klimenko et al., Phys. Rev. **D93**, 042004 (2016).

[41] N. J. Cornish and T. B. Littenberg, Class. Quantum Grav. **32**, 135012 (2015).

[42] J. Veitch et al., Phys. Rev. **D91**, 042003 (2015).

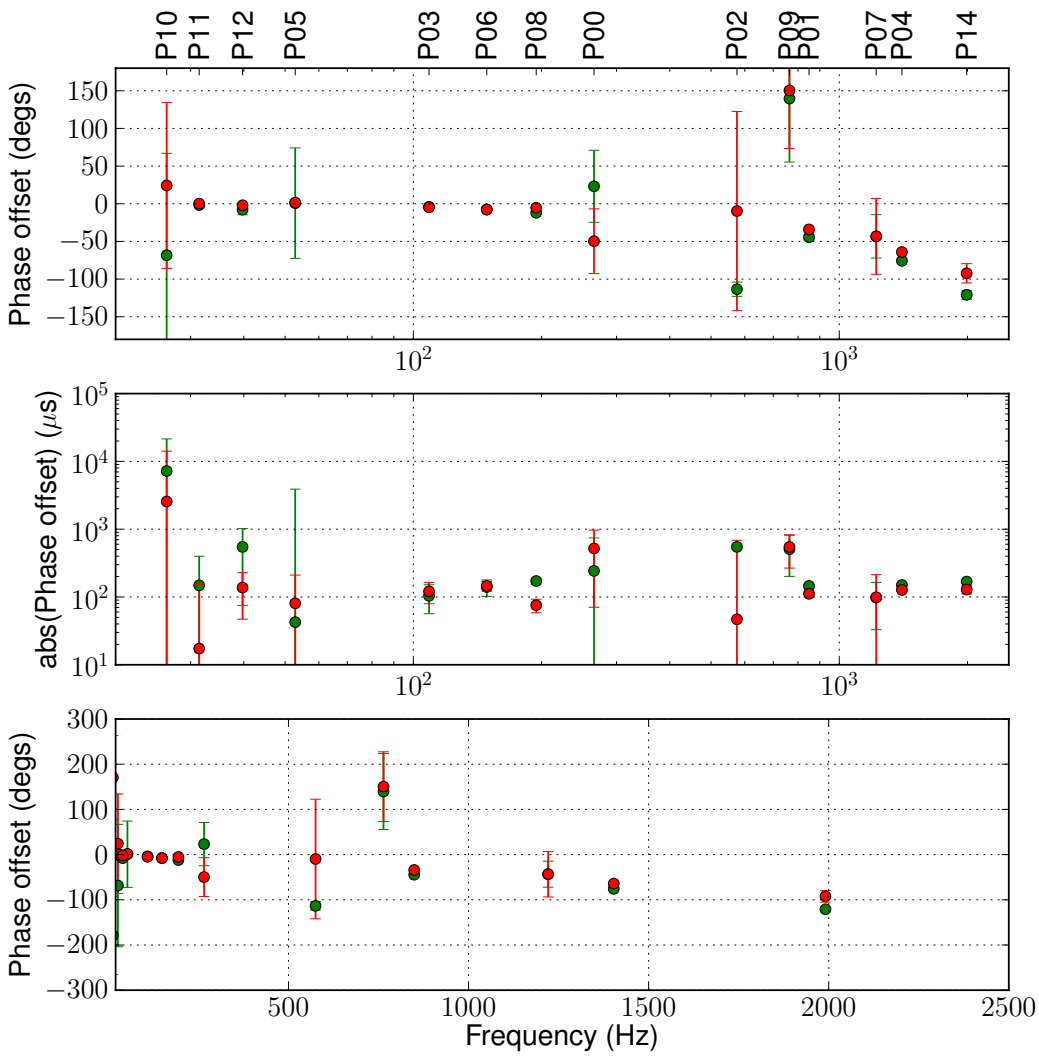

FIG. 14: Comparisons of recovered signal phases for the Hanford and Livingston signals for the 14 recovered continuous-wave injections (P00-P14). *1st panel:* Phase difference (degrees) [recovered minus true]. *2nd panel:* Conversion of phase difference magnitude to time difference. *3rd panel:* Same as 3rd panel but with linear horizontal scale, to indicate the roughly linear dependence of residual phase difference, consistent with a constant uncompensated time delay.

[43] J. Skillings, Bayesian Anal. **1** (2006).
[44] J. Abadie et al. (VIRGO, LIGO), Phys. Rev. **D81**, 102001 (2010).
[45] V. Tiwari, S. Klimenko, V. Necula, and G. Mitselmakher, Class. Quantum Grav. **33**, 01LT01 (2016).
[46] B. Allen and J. D. Romano, Phys. Rev. **D59**, 102001 (1999).
[47] V. Mandic, S. Bird, and I. Cholis (2016), 1608.06699.
[48] J. Aasi et al. (VIRGO, LIGO Scientific), Phys. Rev. Lett. **113**, 231101 (2014).
[49] S. W. Ballmer, Class. Quantum Grav. **23**, S179 (2006).
[50] B. P. Abbott et al. (VIRGO, LIGO), Phys. Rev. Lett. **107**, 271102 (2011).
[51] A. Effler, R. M. S. Schofield, V. V. Frolov, G. Gonzlez, K. Kawabe, J. R. Smith, J. Birch, and R. McCarthy, Class. Quantum Grav. **32**, 035017 (2015).
[52] S. Chatterji, L. Blackburn, G. Martin, and E. Katsavounidis, Class. Quantum Grav. **21**, S1809 (2004).
[53] J. R. Smith, T. Abbott, E. Hirose, N. Leroy, D. Macleod, J. McIver, P. Saulson, and P. Shawhan, Class. Quantum Grav. **28**, 235005 (2011).